



RESEARCH ARTICLE SUMMARY

ATMOSPHERE

Toward a Cenozoic history of atmospheric CO₂The Cenozoic CO₂ Proxy Integration Project (CenCO₂PIP) Consortium

INTRODUCTION: Anthropogenic carbon dioxide (CO₂) emissions have driven an increase in the global atmospheric CO₂ concentration from 280 parts per million (ppm) before industrialization to an annual average of 419 ppm in 2022, corresponding to an increase in global mean surface temperature (GMST) of 1.1°C over the same period. If global CO₂ emissions continue to rise, atmospheric CO₂ could exceed 800 ppm by the year 2100. This begs the question of where our climate is headed. The geologic record is replete with both brief and extended intervals of CO₂ concentration higher than today and thus provides opportunities to project the response of the future climate system to increasing CO₂. For example, it has been estimated that global surface temperature 50 million years ago (Ma) was ~12°C higher than today, in tandem with atmospheric CO₂ concentrations some 500 ppm higher (i.e., more than doubled) than present-day values. Consistent with these estimates, Antarctica and Greenland were free of ice at that time. However, reconstructing these values prior to direct instrumental measurements requires the use of paleoproxies—measurable properties of geological archives that are closely, but only indirectly, related to the parameter in question (e.g., temperature, CO₂). To date,

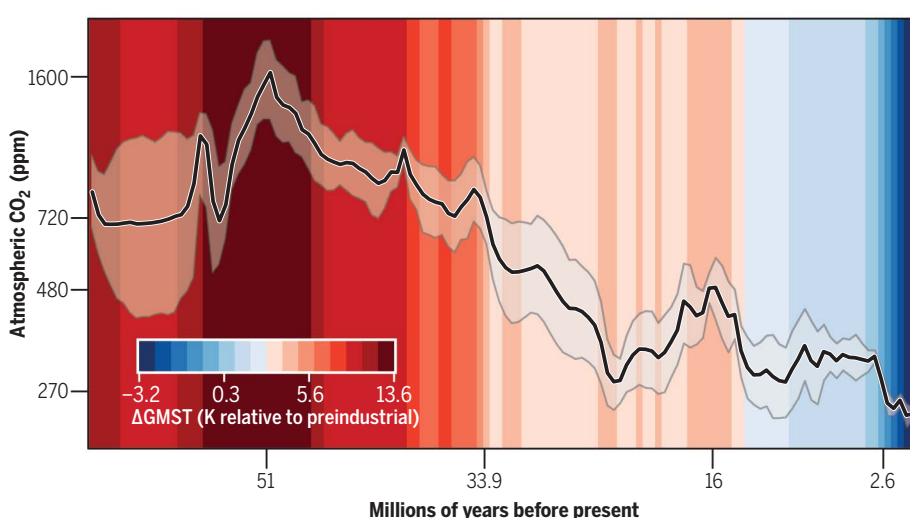
at least eight different proxies from both terrestrial and marine archives have been developed and applied to reconstruct paleo-CO₂, but their underlying assumptions have been revised over time, and published reconstructions are not always consistent. This uncertainty complicates quantification of the climate responses to the ongoing rise of atmospheric CO₂ concentrations.

RATIONALE: Although earlier studies have compiled published paleo-CO₂ estimates, those studies typically applied only limited proxy vetting, included estimates that were made before the proxies were sufficiently validated, and/or focused on only a subset of available proxy data. The international consortium of the Cenozoic CO₂ Proxy Integration Project (CenCO₂PIP) has undertaken a 7-year effort to document, evaluate, and synthesize published paleo-CO₂ records from all available archives, spanning the past 66 million years. The most reliable CO₂ estimates were identified, some records were recalculated to conform with the latest proxy understanding, age models were updated where necessary and possible, and data were categorized according to the community's level of confidence in each estimate. The highest-rated data were eventually combined into a

reconstruction of the Cenozoic history of atmospheric CO₂.

RESULTS: The resulting reconstruction illustrates a more quantitatively robust relationship between CO₂ and global surface temperature, yielding greater clarity and confidence than previous syntheses. The new record suggests that early Cenozoic “hothouse” CO₂ concentrations peaked around 1600 ppm at ~51 Ma. Near 33.9 Ma, the onset of continent-wide Antarctic glaciation coincided with an atmospheric CO₂ concentration of 720 ppm. By ~32 Ma, atmospheric CO₂ had dropped to 550 ppm, and this value coincided with the onset of radiation in plants with carbon-concentrating mechanisms that populate grasslands and deserts today. CO₂ remained below this threshold for the remainder of the Cenozoic and continued its long-term decrease toward the present. Along this trajectory, the middle Miocene (~16 Ma) marks the last time that CO₂ concentrations were consistently higher than at present; Greenland was not yet glaciated at that time, and independent estimates suggest that sea level was some 50 m higher than today. Values eventually dropped below 270 ppm at the Plio-Pleistocene boundary (2.6 Ma), when Earth approached our current “icehouse” state of bipolar glaciation. This and other climatic implications of the revised CO₂ curve, including the evolution of the cryosphere, flora, and fauna, along with the cross-disciplinary data assessment process, are detailed in the full online article.

CONCLUSION: This community-vetted CO₂ synthesis represents the most reliable data available to date and a means to improve our understanding of past changes in global climate and carbon cycling as well as organismal evolution. However, this effort is still incomplete. Data remain sparse during the earlier part of the record and in some instances are dominated by estimates from a single proxy system. Generating a paleo-CO₂ record with even greater confidence will require further research using multiple proxies to fill in data gaps and increase overall data resolution, resolve discrepancies between estimates from contemporaneous proxy analyses, reduce uncertainty of established methods, and develop new proxies. ■



Community-vetted quantitative CO₂ record. Paleo-CO₂ (including 95% credible intervals) is superimposed on the GMST trend over the past 66 million years. Age and CO₂ labels highlight notable climate extrema and transitions as described in the text.

The CenCO₂PIP Consortium authors and affiliations are listed in the full article online.

Corresponding authors: Bärbel Hönisch (hönisch@ldeo.columbia.edu); Dana L. Royer (droyer@wesleyan.edu); Daniel O. Breecker (breecker@jsg.utexas.edu); Gabriel J. Bowen (gabe.bowen@utah.edu); Pratigya J. Polissar (polissar@ucsc.edu); Andy Ridgwell (andy@seao2.org). Cite this article as The CenCO₂PIP Consortium, *Science* **382**, eadi5177 (2023). DOI: [10.1126/science.ad15177](https://doi.org/10.1126/science.ad15177)

S READ THE FULL ARTICLE AT
<https://doi.org/10.1126/science.ad15177>

RESEARCH ARTICLE

ATMOSPHERE

Toward a Cenozoic history of atmospheric CO₂The Cenozoic CO₂ Proxy Integration Project (CenCO₂PIP) Consortium*†

The geological record encodes the relationship between climate and atmospheric carbon dioxide (CO₂) over long and short timescales, as well as potential drivers of evolutionary transitions. However, reconstructing CO₂ beyond direct measurements requires the use of paleoproxies and herein lies the challenge, as proxies differ in their assumptions, degree of understanding, and even reconstructed values. In this study, we critically evaluated, categorized, and integrated available proxies to create a high-fidelity and transparently constructed atmospheric CO₂ record spanning the past 66 million years. This newly constructed record provides clearer evidence for higher Earth system sensitivity in the past and for the role of CO₂ thresholds in biological and cryosphere evolution.

The contribution of atmospheric CO₂ to Earth's greenhouse effect and the potential for variations in the global carbon cycle to cause climate change have been known for more than a century (1), but it was only in 1958 that direct measurements of the concentration of CO₂ in the atmosphere (or molar mixing ratio—the mole fraction of a gas in one mole of air) were systematically collected. Alongside reconstructions of the historical rise in Earth's surface temperature (2), this record has become one of the most influential and scientifically valuable environmental time series, documenting the continuous rise in annual mean CO₂ from 315 parts per million (ppm) in 1958 to 419 ppm in 2022 (3). Projecting beyond these records to estimate how Earth's climate will respond to further increases in CO₂ requires global climate models (4). However, despite successfully explaining observed historical climate change (2), models leave doubt as to whether global mean temperature will rise linearly as a function of future doubling of CO₂ (an invariant "climate sensitivity") or whether climate feedbacks will lead to an increasing (or "state-dependent") sensitivity of climate to CO₂ in the future (5, 6).

We can turn to the geological record to help constrain models and improve our understanding of nonlinearities in the climate system (7), as it documents a variety of global climate changes and, critically, climate states warmer than today. Leveraging this record, however, requires the paired quantification of both past atmospheric CO₂ and temperature. In parallel with recent efforts to compile and vet paleotemperature estimates (8), here we focus on paleo-CO₂ estimates. Samples of an-

cient air can be extracted and analyzed from bubbles preserved in ancient polar ice (9, 10), but continuous ice core records currently only extend our knowledge of CO₂ back about 800 thousand years (kyr) [for a compilation, see (11)], with isolated time slices extending to ~2 Ma (million years ago) (12, 13). Importantly, at no point during the Pleistocene (2.58 Ma to 11,700 years ago) did CO₂ come close to present-day values (419 ppm in the year 2022), with 300 ppm being the highest value measured to date (14). In contrast, depending on the extent of future human emissions, atmospheric CO₂ could reach between 600 and 1000 ppm by the year 2100 (2). Feedbacks between changing climate and the carbon cycle may also amplify or diminish emissions from surficial carbon reservoirs (e.g., thawing permafrost, adjustments in size and composition of the terrestrial biosphere and marine carbon pool), creating additional uncertainty in future CO₂ projections (15, 16). Past changes in CO₂ inherently include the role of these feedbacks, and their study could help reduce uncertainty in Earth system models (17).

A solid understanding of atmospheric CO₂ variation through geological time is also essential to deciphering and learning from other features of Earth's history. Changes in atmospheric CO₂ and climate are suspected to have caused mass extinctions (18, 19) but also evolutionary innovations (20, 21). During the Cenozoic, long-term declines in CO₂ and associated climate cooling have been proposed as the drivers of changing plant physiology (e.g., carbon-concentrating mechanisms), species competition and dominance, and, relatedly, mammalian evolution. A more refined understanding of past trends in CO₂ is therefore central to understanding how modern species and ecosystems arose and may fare in the future.

Extending the CO₂ record beyond the temporally restricted availability of polar ice requires the use of "proxies." In essence, a CO₂ proxy could be any biological and/or geochemical

property of a fossil or mineral that responds to the concentration of ambient CO₂ when it is formed. Unfortunately, unlike in the case of bubbles of ancient air trapped in polar ice, this response is invariably indirect. The connection between a proxy signal and atmospheric CO₂ is often strongly mediated by biological "vital effects" (e.g., concentration of or discrimination against certain molecules, elements, or isotopes as a result of physiological processes such as biomimicry, photosynthesis, respiration), may be indirectly connected to the atmosphere through dissolution of carbon in seawater or lakes, may involve isotopic or other chemical fractionation steps, or a combination of these. When preserved in terrestrial or marine sediments, proxy substrates can also be affected by postdepositional (i.e., diagenetic) processes that must be accounted for. Relationships between proxies and CO₂ are typically calibrated using observations or laboratory experiments; in biological systems, these calibrations are often limited to modern systems (e.g., modern organisms or soils), and applications to the distant past focus on physiologically or physically similar systems preserved in the sediment and rock record (e.g., similar fossil organisms or fossil soils). Most CO₂ proxies also require estimation of one or more additional environmental parameters and hence depend on additional proxy records. The complexity of proxy-enabled paleoclimate reconstructions thus presents a major challenge for creating a self-consistent estimate of atmospheric CO₂ through geological time and requires careful validation.

One of the first paleo-CO₂ proxies to be devised is based on the observation that vascular plants typically optimize the density, size, and opening and closing behavior of stomatal pores on their leaf surfaces to ensure sufficient CO₂ uptake while minimizing water loss (22). A count of stomatal frequencies then provides a simple proxy for the CO₂ concentration experienced by the plant (23). Changes in ambient CO₂ can also drive a cascade of interrelated effects on photosynthesis, the flux of CO₂ into the leaf (largely determined by stomatal size and density), and the carbon isotopic fractionation during photosynthesis ($\Delta^{13}\text{C}$) (22–24). Despite lacking functional stomata, nonvascular plants such as liverworts also exhibit isotopic fractionation during photosynthesis, and their $\delta^{13}\text{C}$ values are thus similarly controlled by ambient CO₂. The list of terrestrial paleo-CO₂ proxies also includes inorganic carbonate nodules precipitated in ancient soils (i.e., paleosols) and sodium carbonate minerals precipitated in continental lacustrine evaporites. Whereas the paleosol proxy uses the carbon isotope composition of carbonate nodules and deconvolves the mixture of atmospheric and soil-respired CO₂ in soil porewaters using models of soil CO₂ (25, 26), the nahcolite

*Corresponding authors: Bärbel Honisch (hoenisch@ldeo.columbia.edu); Dana L. Royer (droyer@wesleyan.edu); Daniel O. Breecker (breecker@jsg.utexas.edu); Gabriel J. Bowen (gabe.bowen@utah.edu); Pratigya J. Polissar (polissar@ucsc.edu); Andy Ridgwell (andy@seas.ox.ac.uk)

†The CenCO₂PIP Consortium authors and affiliations are listed at the end of this paper.

proxy is based on the CO₂ dependence of sodium carbonate mineral equilibria (27, 28). Analogously to nonvascular plants on land, phytoplankton fractionate carbon isotopes during photosynthesis in response to the concentration of dissolved CO₂ in seawater, creating an isotopic signal stored in organic biomolecules that can be retrieved from ocean sediments (29). Boron proxies recorded in fossil shells of marine calcifying organisms are related to seawater pH, which in turn can be related back to atmospheric CO₂ (30, 31). An in-depth discussion of the analytical details, entrained assumptions, and inherent uncertainties of currently available CO₂ proxies, plus summaries of recent advances and opportunities for further validation, is presented in the supplementary materials and in table S1.

Although each of these proxies has been validated extensively, comparing reconstructions from different proxies often reveals discrepancies. Compilations of paleo-CO₂ and explorations of the CO₂-climate linkage already exist (32–34); however, those studies apply limited proxy vetting, include CO₂ estimates that predate major innovations in some methods, and use rather basic data interpolation to assess broad CO₂ trends. Earlier CO₂ reconstructions are also often insufficiently constrained by ancillary data (e.g., concomitant temperature, isotopic composition of seawater or atmosphere) to be consistent with modern proxy theory, have incomplete or missing uncertainty estimates for CO₂ and/or sample age, and may exhibit fundamental disagreement with other proxies, leaving our current understanding of past CO₂ concentrations incomplete.

Here we present the results of a 7-year endeavor by an international consortium of researchers whose collective expertise spans the reconstruction of paleo-CO₂ from all available terrestrial and marine archives. We have jointly created a detailed, open-source database of published paleo-CO₂ estimates including all raw and ancillary data together with associated analytical and computational methods. Each record was vetted and categorized in view of the most recent proxy understanding, with calculations adopting a common methodology including full propagation of uncertainties. We focused our efforts on the Cenozoic, when the spatial distribution of continents and ocean basins, as well as the structure of marine and terrestrial ecosystems, was similar to modern times, yet profound changes in CO₂ and climate occurred. Identifying the most-reliable Cenozoic CO₂ estimates published to date allows us to quantify important physical (e.g., temperature, ice volume) and biological (i.e., physiological, ecosystem) thresholds and tipping points.

We structure this investigation as follows: First we summarize the methodology by which we assessed the CO₂ proxies and associated

estimates. We then apply these methods to derive a series of paleo-CO₂ compilations composed of data with different levels of quality or confidence, and we statistically integrate the “top-tier” data to create a realization of the Cenozoic variability in atmospheric CO₂. This is followed by a discussion of the climatic implications (including climate sensitivity) of the paleo-CO₂ curve and a presentation of an evolutionary perspective. We finish with a road map for further advances in understanding past changes in atmospheric CO₂.

Critical assessment of atmospheric CO₂ proxies

The basis of our synthesis is a set of comprehensive data templates documenting all types of proxy data and their corresponding CO₂ estimates (a total of 6247 data points). The completed data sheets for each study can be accessed as the paleo-CO₂ “Archive” (https://www1.ncdc.noaa.gov/pub/data/paleo/climate_forcing/trace_gases/Paleo-pCO2/) in the National Oceanic and Atmospheric Administration’s National Centers for Environmental Information (NOAA NCEI). These “Archive” sheets report all underlying data at face value from the original publications, but their unprecedented level of detail is designed to facilitate critical evaluation and recalculation of each CO₂ estimate.

From the “Archive,” published CO₂ estimates were evaluated by teams of experts—often including the original authors of the respective data—who are active in validating and applying these proxies. No new proxy data were collected as part of this effort, but estimates were recalculated where needed and possible, and age models were revised where new evidence was readily accessible. Additionally, CO₂ and age uncertainties were updated, as necessary, to consistently reflect propagated 95% confidence intervals (CIs). The vetting criteria are summarized in table S1 and detailed in paleo-CO₂ “Product” sheets (https://www.ncei.noaa.gov/pub/data/paleo/climate_forcing/trace_gases/Paleo-pCO2/product_files/). These CO₂ estimates are categorized as follows: “Category 1” estimates (Fig. 1A; 1673 data points or ~27% of the original total) are based on data whose uncertainty is fully documented and quantifiable in view of current proxy understanding. “Category 2” estimates (Fig. 1B; 1813 data points) contain sources of uncertainty that are not yet fully constrained. These uncertainties vary between proxies and datasets and include, for example, insufficient replication, poorly constrained proxy sensitivity to parameters other than CO₂, or extrapolation of calibration curves. “Category 3” estimates (the residual 2761 data points, or ~44% of the Cenozoic paleo-CO₂ estimates published to date) are either superseded by newer, independently published evaluations from the same raw data or are considered

unreliable owing to factors such as incomplete supporting datasets, which prevent full quantification of uncertainties, or outdated sample preparation methods.

Although objective criteria are applied throughout, the vetting process was particularly challenging for the paleosol- and phytoplankton-based proxies because multiple approaches are currently in use for interpreting these proxy data (35–41). Given the lack of a universally agreed-upon method, we compared multiple approaches for treating the data of these two proxies whenever possible. For the paleosol proxy, the greatest source of uncertainty is in the estimation of paleo-soil CO₂ concentration derived from respiration. Two different approaches are commonly used to estimate paleo-soil CO₂ concentration. The first method is based on proxy-estimated mean annual rainfall, whereas the second is based on soil order (i.e., the most general hierarchical level in soil taxonomy, comparable to kingdom in the classification of biological organisms). However, few records in the database allow for a direct comparison between the two approaches. An opportunity for comparison exists with two Eocene records (37, 42), where recalculation using each of the two different methods leads to CO₂ estimates that do not overlap within 95% CIs for most stratigraphic levels (fig. S6). This implies that the uncertainty in estimating paleo-soil CO₂ concentration derived from respiration cannot be fully quantified with either of these approaches. Thus, most paleosol-based CO₂ estimates were designated as Category 2. For the phytoplankton proxy, routinely applied methods differ in how algal cell size and growth rate are accounted for, as well as the assumed sensitivity of algal δ¹³C values to aqueous CO₂ concentration (see supplementary materials for details). Where data were available, we compared both newer and traditional methods, finding that although there are deviations between the resulting CO₂ estimates, they do agree within 95% CIs. We hence assign many phytoplankton CO₂ estimates to Category 1 and present mean CO₂ and uncertainty values that reflect the range of results from the different methods.

Toward a Cenozoic history of atmospheric CO₂

Our composite Category 1 and 2 realizations of Cenozoic CO₂ (Fig. 1, A and B) display much better agreement among proxies than does the raw, uncurated collection (“Archive,” Fig. 1C). Encouragingly, objective criteria applied to the original data products automatically placed the earlier-reported estimates of “negative” CO₂, as well as some unusually high values, into Category 3, and without subjective intervention to otherwise filter them. We note that the Category 1 composite is now largely dominated by marine proxy estimates, with some intervals (e.g., the middle Paleocene, ~63 to

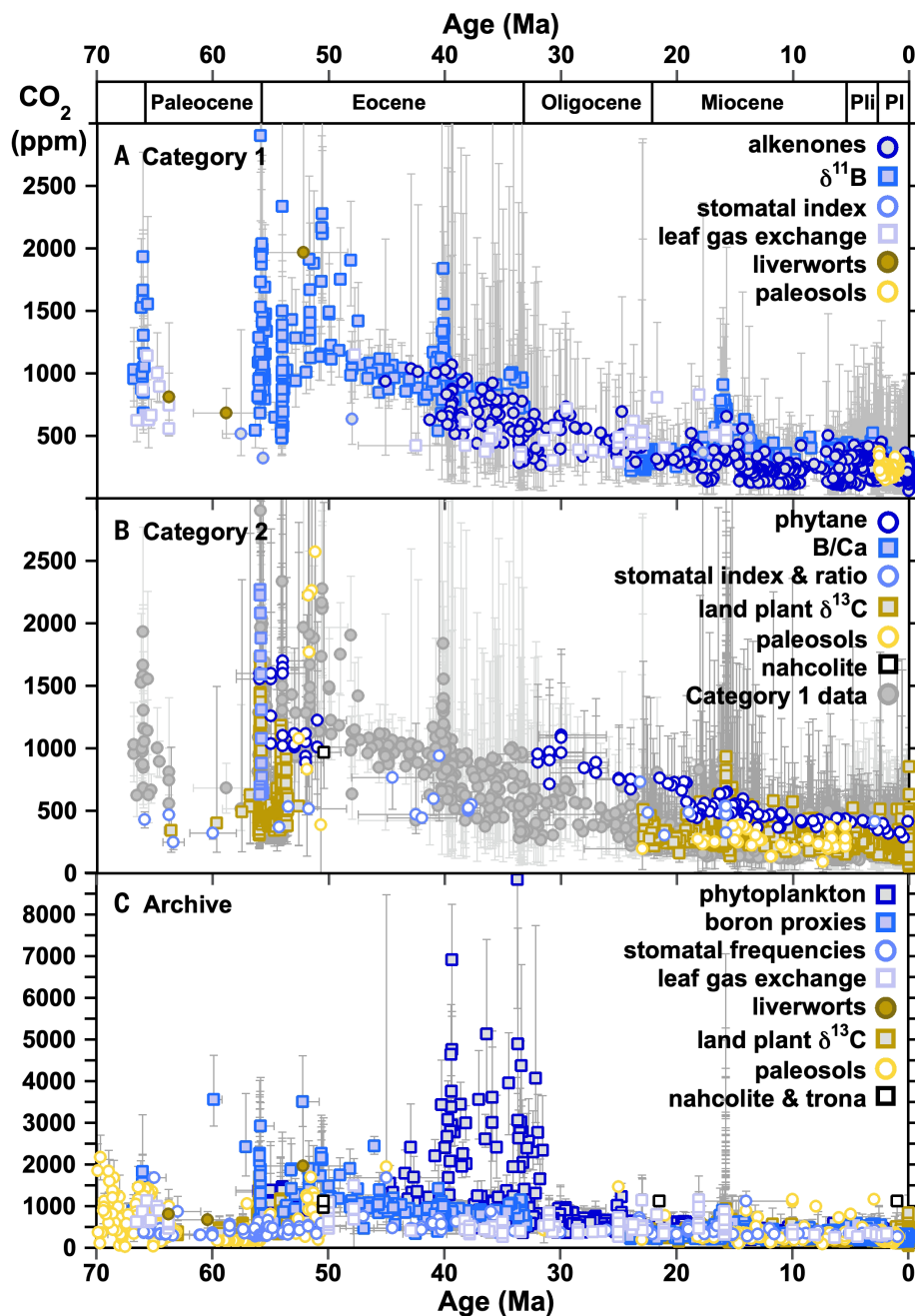


Fig. 1. Documentation and assessment of all Cenozoic paleo-CO₂ estimates published to date.

Individual proxy estimates, as defined by the colored symbols in the legends. (A) Vetted Category 1 estimates with their fully developed uncertainty estimates (95% CIs); age uncertainties have been updated or established to the best of current understanding. (B) Vetted Category 2 estimates whose uncertainty is not yet fully constrained. Category 1 data are shown in gray for reference. (C) Archive compilation of all CO₂ estimates in their originally published quantification. To toggle view of individual proxy records in (A) and (C), please go to <https://paleo-co2.org/>. Pli., Pliocene; Pl., Pleistocene.

57 Ma) very sparsely sampled. Furthermore, some intervals (e.g., Oligocene, Miocene) still exhibit notable differences between proxies; for instance, marine-based CO₂ estimates start high and decline during the Oligocene (~34 to 23 Ma), whereas plant-based estimates suggest overall lower and constant CO₂ (Fig. 1A). Estimates of

global temperature (Fig. 2B) during this time interval are largely invariant, which leaves us with the question of whether CO₂ and climate were decoupled during this interval, or whether there is a systematic bias in the marine or plant-based CO₂ proxies and/or in the temperature proxies. All proxy-based estimates become more

uncertain further back in time as our knowledge of vital effects in biological proxy carriers, secular changes in the elemental and isotopic composition of ocean and atmosphere, and proxy sensitivity to environmental parameters that change along with CO₂ (e.g., temperature, rainfall; see supplementary materials for details) becomes less certain. In some cases, ancillary constraints and uncertainties are shared across multiple proxies (e.g., assumed atmospheric δ¹³C is common to proxies based on land plant δ¹³C, leaf gas exchange, and paleosols), creating interdependence of estimates from seemingly independent proxies. More robust paleo-CO₂ reconstruction thus requires not only continued application of all proxies but also replication from different locations.

Although some uncertainties and proxy disagreements remain, the much-improved agreement within the vetted paleo-CO₂ compilation gives us confidence that a quantitative reconstruction of Cenozoic CO₂ based on the combined Category 1 data is possible. To do so, we statistically model mean CO₂ values at 500-kyr intervals, together with uncertainties in age and proxy CO₂ estimates (Fig. 2A; see supplementary materials for details). Our choice of a 500-kyr resolution interval reflects a compromise driven by the proxy data compilation. Although parts of the Cenozoic, particularly the Plio-Pleistocene, are sampled at higher temporal resolution, the density of records remains relatively sparse throughout much of the Paleogene (1 datum per 190 kyr on average). As a result, the data (and in some cases the underlying age models) are not suited to interpreting higher-frequency (e.g., Milankovitch-scale) variations in atmospheric composition, and we focus here on low-frequency (e.g., multi-million year) trends and transitions. Proxy sampling within some intervals may be biased toward conditions that deviate from the 500-kyr mean [most notably here, the Paleocene-Eocene Thermal Maximum (PETM)]. We do not attempt to remove this bias but instead recommend caution in interpreting any features expressed at submillion-year timescales.

This curve (Fig. 2A) allows us to constrain Cenozoic paleo-CO₂ and its uncertainty with greater confidence than earlier efforts. The highest CO₂ values of the past 66 Myr appear during the Early Eocene Climatic Optimum (EECO; ~53 to 51 Ma), whereas the lowest values occur during the Pleistocene. In contrast to earlier compilations, which suggested early Cenozoic CO₂ concentrations of <400 ppm (33), rigorous data vetting and newly published records place early Paleocene mean CO₂ in our reconstruction between 650 and 850 ppm. However, the Paleocene remains data-poor, and uncertainty in the curve remains large. Although the Paleocene record is predominantly based on the boron isotope proxy (Fig. 1A), inclusion of other (nonmarine) proxy data does

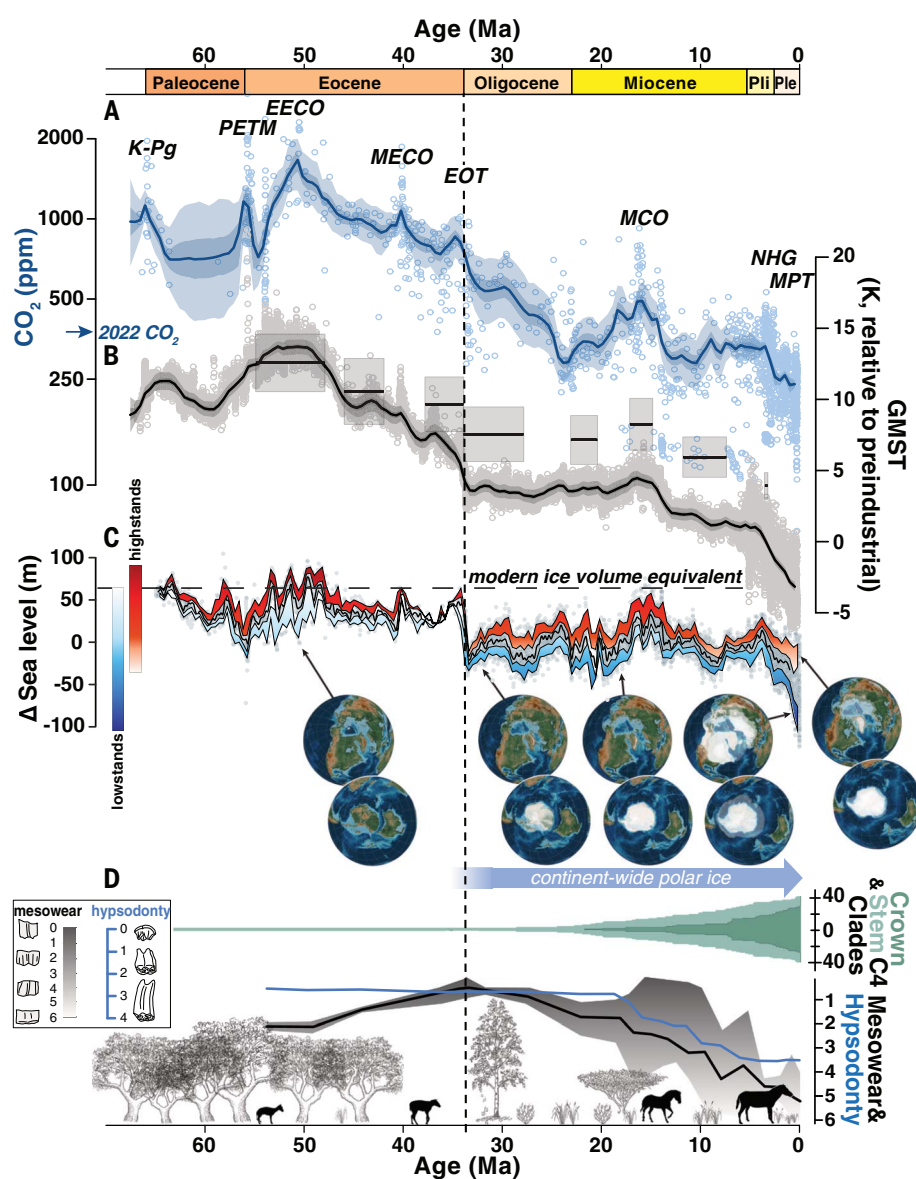


Fig. 2. Category 1 paleo-CO₂ record compared to global climate signals. The vertical dashed line indicates the onset of continent-wide glaciation in Antarctica. (A) Atmospheric CO₂ estimates (symbols) and 500-kyr mean statistical reconstructions (median and 50 and 95% credible intervals; dark and light-blue shading, respectively). Major climate events are highlighted: K-Pg, Cretaceous/Paleogene boundary; PETM, Paleocene Eocene Thermal Maximum; EECO, Early Eocene Climatic Optimum; MECO, Middle Eocene Climatic Optimum; EOT, Eocene/Oligocene Transition; MCO, Miocene Climatic Optimum; NHG, onset of Northern Hemisphere Glaciation; and MPT, Mid-Pleistocene Transition. The 2022 annual average atmospheric CO₂ of 419 ppm is indicated for reference. (B) Global mean surface temperatures estimated from benthic $\delta^{18}\text{O}$ data following Westerhold *et al.* (43) (solid line, individual proxy estimates as symbols, and statistically reconstructed 500-kyr mean values shown as the continuous curve, with 50 and 95% credible intervals) and from surface temperature proxies (gray boxes) (45). (C) Sea level after (66) with gray dots displaying raw data; the solid black line reflects median sea level in a 1-Myr running window. High- and lowstands are defined within a running 400-kyr window, with lower and upper bounds of highstands defined by the 75th and 95th percentiles, and lower and upper bounds of lowstands defined by the 5th and 25th percentiles in each window. Globes depict select paleogeographic reconstructions and the growing presence of ice sheets in polar latitudes from (116). (D) Crown ages show that C₄ clades, with CCMs adapted to low CO₂, initially diversified in the early Miocene, and then rapidly radiated in the late Miocene (117). Flora transition from dominantly forested and woodland to open grassland habitats based on fossil phytolith abundance data (96). North American equids typify hooved animal adaptations to new diet and environment (103), including increasing tooth mesowear (black line; note the inverted scale), hypsodonty (blue line), and body size.

influence and refine the reconstruction through this epoch, supporting the value of the multi-proxy approach (fig. S10). After the rapid CO₂ rise and fall associated with the PETM at 56 Ma, mean CO₂ steadily rose to peak values of ~1600 ppm around 51 Ma during the EECO. The middle and late Eocene recorded slightly lower values (800 to 1100 ppm). Mean CO₂ dropped to <600 ppm across the Eocene-Oligocene transition (EOT; 33.9 Ma) and reached values that generally fall between ~400 and 200 ppm during the Miocene through Pleistocene, except for a notable increase during the Middle Miocene (~17 to 15 Ma) to a mean of ~500 ppm. Uncertainty in the mean CO₂ values drops substantially in the Plio-Pleistocene (fig. S11), as expected given a drastic increase in data density. Our analysis suggests that ~14.5 to 14 Ma was the last time the 500-kyr-mean CO₂ value was as high as it is at present (fig. S11) and that all Plio-Pleistocene peak interglacial CO₂ concentrations were exceptionally likely to be less than those of the modern atmosphere (fig. S12). In contrast, before the Miocene, there is very little support (<2.5% probability) for Cenozoic 500-kyr-mean CO₂ values reaching or falling below preindustrial levels.

Climatic implications of the revised CO₂ curve

Relationship with global temperature change and climate sensitivity

Our reconstructed Cenozoic CO₂ trends are broadly coherent with those for global temperature as inferred, for instance, from the oxygen isotopic composition ($\delta^{18}\text{O}$) of fossil benthic foraminifera shells (43, 44) and compilations of global surface temperature (45) (Fig. 2B). The Paleocene and Eocene epochs display overall higher temperatures and atmospheric CO₂ concentrations as compared with the later Oligocene, Miocene, and Pliocene—consistent with a predominantly greenhouse gas-regulated global energy budget. More specifically, the slow rise and subsequent fall of CO₂ over the course of the Paleocene and Eocene are mirrored by global temperatures, just as a transient Miocene CO₂ rise coincides with a period of warming at the Miocene Climatic Optimum (MCO). The EOT is identifiable in both the CO₂ and temperature records, despite the smoothing introduced by the curve fitting and 500-kyr binning interval.

Despite this overall agreement, rates and timing of CO₂ are not always synchronized with temperature changes in the two records (Fig. 2, A and B). For example, CO₂ appears broadly static or even rising during the late Eocene (37 to 34 Ma) and late Miocene (11 to 5 Ma) despite global cooling at these times (46). Conversely, decreasing CO₂ during the early Oligocene corresponds with relatively stable global temperatures [Fig. 2B, but see also (47, 48)] and ice volume (Fig. 2C) at that time.

We note that the reconstructed Oligocene CO₂ decrease is driven by the contribution of marine proxies to the composite curve, whereas estimates from leaf gas exchange proxies are low and broadly static (Fig. 1C), a discrepancy that cannot be resolved without further experimentation and data collection. We caution that, even at the 500-kyr resolution of our study, the relative timing of CO₂ and temperature change might be unresolved in poorly sampled intervals (i.e., middle Paleocene) but should be well resolved during more-recent, well-sampled intervals (i.e., late Miocene through present; fig. S8). Is the occasional divergence of temperature and CO₂ change evidence for occasional disconnects between CO₂ forcing and climate response? Although one might posit bias in the CO₂ reconstruction, the strength of our multiproxy approach is the reduced likelihood that multiple proxies exhibit common bias during particular periods of the Cenozoic. We suggest that some cases of divergence between temperature and CO₂ could reflect non-CO₂ effects on climate [e.g., changes in paleogeography affecting ocean circulation, albedo, and heat transport (49)], or the temperature reconstructions used herein could be biased by nonthermal influences [e.g., uncertain elemental and isotopic composition of paleoseawater, physiological or pH effects on proxies (48, 50)].

Our updated CO₂ curve, in conjunction with existing global temperature reconstructions, gives us the opportunity to reassess how climate sensitivity might have evolved through the Cenozoic. The most commonly reported form of climate sensitivity is equilibrium climate sensitivity (ECS), which focuses on fast feedback processes (e.g., clouds, lapse rate, snow, sea ice) and is therefore best suited for predicting present-day warming [$\sim 3^{\circ}\text{C}$ for a doubling of CO₂ above the preindustrial condition (2)]. Because the average temporal resolution of our CO₂ database is coarser than 1000 years, we cannot estimate ECS directly. Instead, our data are most appropriate for interpreting an Earth system sensitivity [ESS_[CO₂]], following the taxonomy of (51)—the combination of short-term climate responses to doubling CO₂ plus the effects of slower, geological feedback loops such as the growth and decay of continental ice sheets. We compare our reconstructed 500-kyr-mean CO₂ values with two different estimates of global surface temperature. We apply the same Bayesian inversion model used in the CO₂ reconstruction to derive 500-kyr-mean surface temperatures from the benthic foraminiferal δ¹⁸O compilation of (43), which we convert to temperatures using the methodology of (44) (Fig. 2B). In addition, we pair a set of multiproxy global surface temperature estimates for eight Cenozoic time intervals (Fig. 2B) (45) with posterior CO₂ estimates from time bins corresponding to each

interval. The two temperature reconstructions are broadly similar, although the benthic record suggests relatively higher temperatures during the hothouse climate of the Paleocene and Eocene, whereas the multiproxy reconstruction is elevated relative to the benthic record during the Oligocene and Neogene.

The coevolution of atmospheric CO₂ and global mean surface temperature (GMST) over the Cenozoic is shown in Fig. 3. Because CO₂ is on a log scale, the slopes of lines connecting two adjacent points in time reflect the average intervening ESS_[CO₂]. Benthic δ¹⁸O-derived tem-

peratures suggest that early Paleocene warming occurs with a very high ESS_{[CO₂] > 8°C per CO₂ doubling), although CO₂ uncertainties are large during this time interval. ESS_{[CO₂] steadily declines toward the peak of Cenozoic warmth at ~50 Ma, then steepens again to ~8°C per CO₂ doubling for much of the cooling through to the EOT at ~34 Ma. In contrast, the multiproxy global temperature record suggests a lower ESS_{[CO₂] of ~5°C between the early Eocene and earliest Oligocene. During the Oligocene and early part of the Miocene, both temperature records imply a near-zero ESS_[CO₂].}}}

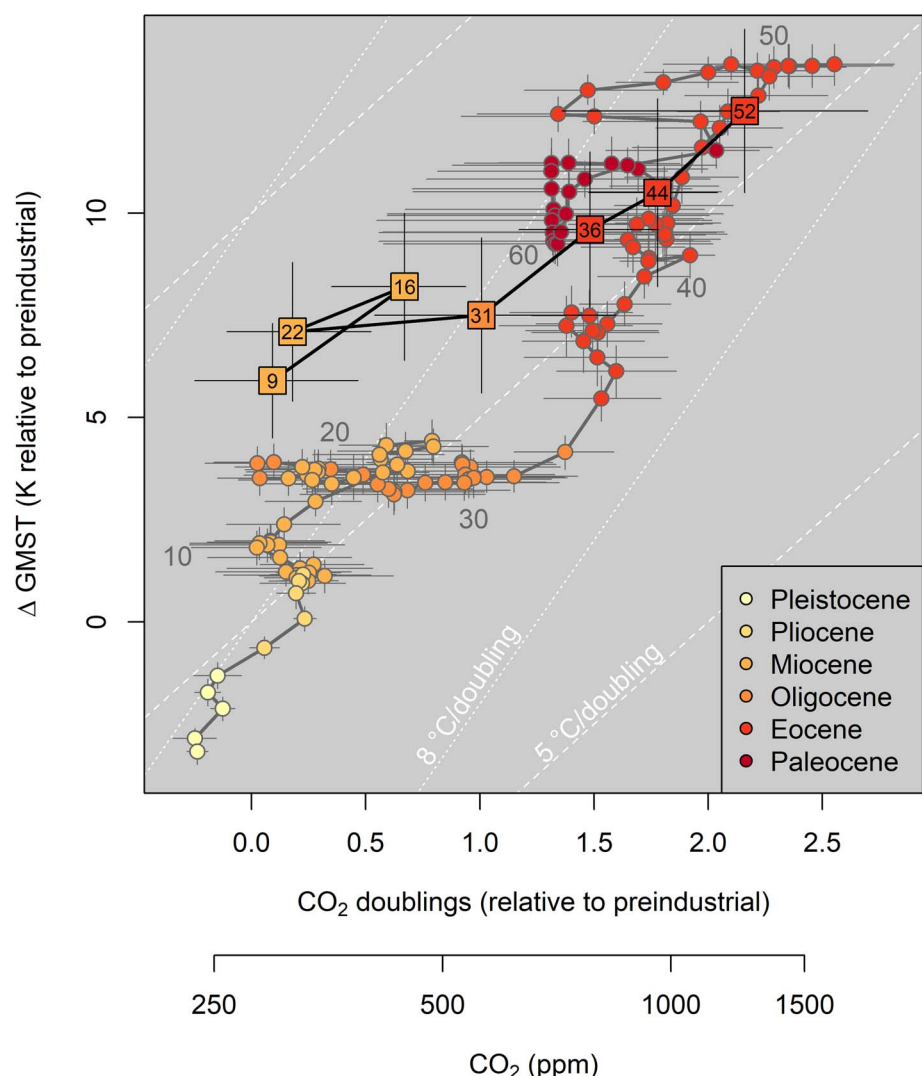


Fig. 3. Application of the Category 1 CO₂ record to determine ESS_[CO₂]. GMST deviation (kelvin) from preindustrial global average surface temperature of 14.15°C is displayed versus paleo-CO₂ doublings relative to the preindustrial baseline of 280 ppm (upper x axis) and paleo-CO₂ estimates on a log scale (lower x axis). The slopes between two points in time reflect the average ESS_[CO₂]. Circles reflect 500-kyr binned Category 1 CO₂ estimates paired with corresponding GMST means from (43); squares pair CO₂ and GMST means from compilations of sea surface temperature (45) in seven coarsely resolved time intervals. Note that this figure omits the Pliocene temperature estimate of (45) because it samples too short a time interval (compare with Fig. 2) to be comparable with mean CO₂. Data from Cenozoic epochs are color coded and shift from red (Paleocene) to yellow (Pleistocene); labels indicate specific age bins (Ma). Dashed lines indicate reference ESS_{[CO₂] lines of 8° and 5°C warming per doubling of CO₂.}

meaning that CO₂ values appear to decline with no appreciable global cooling. ESS_[CO₂] implied by both temperature reconstructions steepens again from the middle Miocene (~16 Ma) to present, averaging 8°C per CO₂ doubling over the past 10 Myr.

An alternative perspective on early Cenozoic climate forcing was introduced by (44), who hypothesized that all pre-Oligocene climate change was the response of direct and indirect CO₂ radiative forcing plus long-term change in solar output (i.e., constant albedo). Consequently, they converted Paleocene and Eocene benthic δ¹⁸O-derived GMST to estimates of CO₂ change required to explain the temperature record. Our reconstruction offers a direct test of this hypothesis, and although it compares well with the δ¹⁸O approach of (44) throughout much of the early Cenozoic, our curve suggests that the late Eocene decline in CO₂ was less severe than expected under the constant albedo assumption (fig. S13). This result is consistent with a growing contribution of glacier and sea ice albedo effects (52, 53) and the opening of Southern Ocean gateways (54) to climate cooling preceding the Eocene-Oligocene boundary.

In summary, the Cenozoic compilation confirms a strong link between CO₂ and GMST across timescales from 500 kyr to tens of millions of years, with ESS_[CO₂] generally within the range of 5° to 8°C—patterns consistent with most prior work (32–34, 45, 51, 55–60) and considerably higher than the present-day ECS of ~3°C. Both temperature reconstructions imply relatively high ESS_[CO₂] values during the last 10 Myr of the Cenozoic, when global ice volumes were highest. This agrees with expectations of an amplified ESS_[CO₂] due to the ice-albedo feedback (61). However, even during times with little to no ice (Paleocene to early Eocene), we find elevated values of ESS_[CO₂] (approaching or exceeding 5°C per CO₂ doubling). This implies that fast, non-ice feedbacks, such as clouds or non-CO₂ greenhouse gases (60, 62–65), were probably stronger in the early Paleogene than they are in the present-day climate system (5). The Oligocene to early Miocene is the most enigmatic interval, with an apparent decrease in CO₂ despite relatively stable temperature, implying near-zero ESS_[CO₂]. It should be noted that this is one interval where different CO₂ proxies disagree on CO₂ change (Fig. 1A), with relatively stable values from plants but a decline in values from alkenones. More work is needed to confirm these CO₂ and temperature findings, but if these estimates are correct, this could partly reflect transition from a climate state too cold to support the strong, fast feedbacks (e.g., clouds) of the early Eocene (5) but not cold enough to generate strong ice-albedo feedback. Tectonic changes in the arrangement of continents and the opening of critical ocean gateways may also be confounding derivation of ESS_[CO₂] at that time (49, 54).

Relationship with the evolution of the cryosphere

Our composite CO₂ record also enables reexamination of the evolution of Earth's cryosphere (Fig. 2C) in relation to CO₂ radiative forcing. We use the sea level estimation of (66) for this comparison because it covers the entire Cenozoic and is somewhat independent of the benthic δ¹⁸O stack (43) used for the GMST derivation in Fig. 2B and also of the more recent sea level reconstruction of (67). Although there are substantial differences between the two sea level estimates, the main features discussed herein are broadly consistent between them. The establishment of a permanent, continent-wide Antarctic ice shield at the EOT (~34 Ma) comes at the end of a ~10-Myr period of generally slowly decreasing CO₂. There is evidence for isolated, unstable Antarctic glaciers at various points during the 10-Myr interval preceding the EOT (50, 53, 66, 68), which is consistent with the increasing paleogeographic isolation of Antarctica and Southern Ocean cooling (54), and CO₂ may have been sufficiently low to enable the repeated crossing of a glaciation threshold by periodic orbital forcing. Tectonic cooling of Antarctica would have progressively raised the CO₂ glaciation threshold, which has been modeled to be between 560 and 920 ppm (69, 70). Our composite CO₂ record allows us to further assess this glaciation threshold but requires determining the point during glacial inception when strong positive feedbacks (e.g., ice-albedo and ice sheet elevation) commenced and ice sheet growth accelerated (71). Using the sea level curve of (66), we determine this point to be 33.75 ± 0.25 Ma, where our composite CO₂ record suggests 719⁺¹⁸⁰₋₁₅₂ ppm (95% CIs). Once established, the land-based Antarctic ice sheet likely persisted for the remainder of the Cenozoic, although substantial retreat of land-based ice has been modeled (30 to 36 m sea level equivalent) (72) and estimated from proxies (Fig. 2C) for the MCO. During the MCO, 500-kyr-mean CO₂ values increased to ~500 ppm (Fig. 2A and fig. S10), and benthic foraminiferal δ¹⁸O (Fig. 2B) (43) and clumped isotopes (50) indicate warming. Although the stability of the land-based Antarctic ice sheet depends on many factors in addition to CO₂-induced global warming [e.g., hysteresis (73) and bed topography (74)], our composite record indicates that considerable retreat of land-based ice did not occur below 441 to 480 ppm (2.5th to 50th percentiles), and some land-based ice may have persisted up to 563 ppm (97.5th percentile) during the MCO. Excepting the MCO, atmospheric CO₂ has remained below our current value of 419 ppm since the late Oligocene (Fig. 2A and fig. S10), with relatively small sea level variations [up to ~20 m; Fig. 2C and (67)] being driven by orbitally forced melting of the marine-based ice sheet (72, 75). Finally, at

~2.7 Ma, the transition to intensified Northern Hemisphere glaciation and orbitally driven glacial cycles coincided with CO₂ values that began decreasing after a relative high during the Pliocene (Fig. 2A).

Evolutionary implications of the revised CO₂ curve

Whereas geologic trends in terrestrial floral and faunal habitat ranges (76, 77) and diversity (78–80) are largely thought to be controlled by temperature and associated climate patterns, atmospheric CO₂ has been hypothesized to drive the evolution of biological carbon-concentrating mechanisms (CCMs) and their subsequent diversification in terrestrial plants (Fig. 2D) (81, 82). Our realization of how atmospheric CO₂ has varied through the Cenozoic allows us to re-examine this hypothesis. The two primary CCMs in terrestrial plants are the crassulacean acid metabolism (CAM) and C₄ photosynthetic syndromes. CCMs in terrestrial C₄ and CAM plants confer competitive advantages over the ancestral C₃ pathway under higher growing season temperatures, low rainfall, and lower atmospheric CO₂. As a result, C₄ photosynthesis contributes about 23% of today's global terrestrial gross primary production (83).

Plant clades with the C₄ pathway first emerged in the early Oligocene (84, 85), yet they did not expand to ecological significance until the late Miocene [i.e., they contributed <5% of gross primary production before ~10 Ma; Fig. 2D and (86–88)]. CAM plants (e.g., cacti, ice plants, agaves, and some orchids) underwent substantial diversification events around the late Oligocene and late Miocene (89–91). Taken together, two general biological thresholds emerge from our CO₂ record: (i) All known origins of C₄ plants occurred when atmospheric CO₂ was lower than ~550 ppm [i.e., after 32 Ma; Fig. 2, A and D, and (84)], which is in agreement with theoretical predictions (92, 93). (ii) All major Cenozoic CAM diversification events coincided with intervals when CO₂ was lower than ~430 ppm (i.e., after 27 Ma) (89, 90). Our record is thus consistent with decreasing atmospheric CO₂ (<550 ppm) being a critical threshold for the Cenozoic origin, diversification, and expansion of C₄ and CAM plants within grasslands, arid habitats (such as deserts), and habitats (such as epiphytes), and provides strong data support for previous hypotheses (20, 84, 86, 88, 89, 92, 94, 95). Notably, after their origin in the early Oligocene, C₄ plants did not immediately proliferate. By ~24 to ~18 Ma, open habitat grasslands are evident on most continents (96), yet widespread dispersal of C₄ plants was delayed until the late Miocene and without any apparent decline in CO₂ (Fig. 2D). Therefore, the rise of C₄ plants to their dominance in many tropical and subtropical ecosystems was likely driven (and is maintained today) by other factors,

such as fire, seasonality of rainfall, and herbivory (i.e., grazing that keeps landscapes open) (97, 98). The temporal evolution of these factors warrants further study as we move toward a future where CO₂ may rise above the 550-ppm threshold that was key to the origin, taxonomic diversification, and spread of C₄ plants.

Terrestrial mammals evolved and adapted to the changing and more-open floral ecosystems of the late Cenozoic (99–101) and are thus indirectly linked to the 550-ppm atmospheric CO₂ threshold discovered herein. In particular, dental wear patterns (such as the shape of the chewing surface of a tooth, i.e., mesowear) and tooth morphology, such as crown height, reflect an increasingly abrasive and tough diet (102, 103) and can be traced across many herbivore lineages during this period. For instance, mesowear in North American Equidae (horses and their ancestors) (Fig. 2D) began to increase in the late Eocene and steadily continued to increase into the Quaternary. Similarly, equids evolved high-crowned (hypodont) teeth in the Miocene (103–105), and their body size increased to accommodate higher intake of more-abrasive, grassy vegetation (Fig. 2D).

Evolutionary trends are a little less clear in the ocean, because marine algal CCMs are ubiquitous and diverse in form (106) and are believed to have an ancient origin. Moreover, the large spatial and seasonal variance of dissolved CO₂ in the surface ocean (as compared with the relatively uniform seasonal and spatial concentration of CO₂ in the air) may somewhat decouple their evolution from geologic trends in atmospheric CO₂. Evidence exists that marine algae, and in particular the coccolithophores (i.e., the source of the alkenone biomarkers), express CCMs to a greater extent when CO₂ is lower (107–109), with estimates of cellular carbon fluxes suggesting that enhanced CCM activity in coccolithophores began between ~7 and 5 Ma (110). However, our revised CO₂ curve displays mean atmospheric CO₂ broadly constant at 300 to 350 ppm since at least ~14 Ma (Fig. 2A and fig. S10), suggesting that increased CCM activity may reflect other proximal triggers, perhaps involving changes in ocean circulation and nutrient supply.

Perspectives and opportunities for further advances

Our community-assessed composite CO₂ record and statistically modeled time-averaged CO₂ curve exhibit greater clarity in the Cenozoic evolution of CO₂ and its relationship with climate than was possible in previous compilations and furthermore highlight the value of cross-disciplinary collaboration and community building. Generating a paleo-CO₂ record with even greater confidence requires targeted efforts using multiple proxies to fill in data gaps, higher resolution and replication from multiple locations, and novel approaches to

resolve remaining differences between CO₂ proxy estimates. Specifically, although the number and diversity of paleo-CO₂ proxy records continue to grow, data remain relatively sparse during several key parts of the Cenozoic record (e.g., middle Paleocene, Oligocene). Moreover, records from the Paleocene and Eocene are dominated by estimates from the boron isotope proxy, increasing the potential for bias. Targeted efforts are hence needed to expand the number and diversity of data through these intervals and to refine multiproxy reconstructions. Additionally, despite substantial progress, there remains a lack of consensus regarding the identity and/or quantification of some of the factors underlying each of the proxy systems analyzed here. New experimental and calibration studies, particularly those that isolate and quantify specific mechanistic responses and/or their interactions, need to be undertaken to reduce potential biases and uncertainty for each method. For instance, the emerging fields of genomics, evolutionary and developmental biology, and proteomics provide exciting opportunities for improving and understanding paleo-proxy systematics. Furthermore, and associated with improved experimental quantification, refining our theoretical and mechanistic understanding of how proxies are encoded will allow us to create explicit and self-consistent representations of the processes involved. The development of proxy system forward models provides a promising leap in this direction (111). Bayesian statistical methods can then enable the full suite of models and data to be integrated and constrain the range of environmental conditions, including atmospheric CO₂ and other variables that are consistent with the multiproxy data (112, 113). Finally, development of new proxies is also a realistic and desirable aim. For instance, while this study focuses on more established proxies, new proxies such as coccolith calcite stable isotopes (114) and mammalian bone and teeth oxygen-17 anomalies (115) show promising results for reconstructing paleo-CO₂ but perhaps require further validation before they can be assessed with confidence.

Proxies and proxy-based reconstructions of how atmospheric CO₂ has varied through deep time have improved immeasurably over the past few decades. Although they will never allow us to reconstruct past CO₂ with the same fidelity as direct air measurement, our study shows how community-based consensus assessment, together with a critical reanalysis of proxy models and assumptions, can progressively move us toward a quantitative history of atmospheric CO₂ for geological time.

REFERENCES AND NOTES

- S. Arrhenius, XXXI. On the influence of carbonic acid in the air upon the temperature of the ground. *Lond. Edinb. Dublin Philos. Mag. J. Sci.* **41**, 237–276 (1896). doi: 10.1080/14786449608620846
- IPCC, *Climate Change 2021: The Physical Science Basis. Contribution of Working Group I to the Sixth Assessment Report of the Intergovernmental Panel on Climate Change*, V. Masson-Delmotte et al., Eds. (Cambridge Univ. Press, 2021).
- P. Tans, R. Keeling, “Carbon cycle greenhouse gases: Trends in atmospheric carbon dioxide” (National Oceanic and Atmospheric Administration, Earth System Research Laboratories, Global Monitoring Laboratory, 2023); www.esrl.noaa.gov/gmd/ccgg/trends/.
- K. E. Taylor, R. J. Stouffer, G. A. Meehl, An overview of CMIP5 and the experiment design. *Bull. Am. Meteorol. Soc.* **93**, 485–498 (2011). doi: 10.1175/BAMS-D-11-00094.1
- R. Caballero, M. Huber, State-dependent climate sensitivity in past warm climates and its implications for future climate projections. *Proc. Natl. Acad. Sci. U.S.A.* **110**, 14162–14167 (2013). doi: 10.1073/pnas.1303365110; pmid: 23918397
- J. Zhu, C. J. Poulsen, On the increase of climate sensitivity and cloud feedback with warming in the community atmosphere models. *Geophys. Res. Lett.* **47**, e2020GL089143 (2020). doi: 10.1029/2020GL089143
- J. Zhu, C. J. Poulsen, B. L. Otto-Biesner, High climate sensitivity in CMIP6 model not supported by paleoclimate. *Nat. Clim. Chang.* **10**, 378–379 (2020). doi: 10.1038/s41558-020-0764-6
- E. J. Judd et al., The PhanST global database of Phanerozoic sea surface temperature proxy data. *Sci. Data* **9**, 753 (2022). doi: 10.1038/s41597-022-01826-0; pmid: 36473888
- R. J. Delmas, J.-M. Ascencio, M. Legrand, Polar ice evidence that atmospheric CO₂ 20,000 yr BP was 50% of present. *Nature* **284**, 155–157 (1980). doi: 10.1038/284155a0
- A. Neftel, H. Oeschger, J. Schwander, B. Stauffer, R. Zumbrunn, Ice core sample measurements give atmospheric CO₂ content during the past 40,000 yr. *Nature* **295**, 220–223 (1982). doi: 10.1038/295220a0
- B. Bereiter et al., Revision of the EPICA Dome C CO₂ record from 800 to 600 kyr before present. *Geophys. Res. Lett.* **42**, 542–549 (2015). doi: 10.1002/2014GL061957
- Y. Yan et al., Two-million-year-old snapshots of atmospheric gases from Antarctic ice. *Nature* **574**, 663–666 (2019). doi: 10.1038/s41586-019-1692-3; pmid: 31666720
- J. A. Higgins et al., Atmospheric composition 1 million years ago from blue ice in the Allan Hills, Antarctica. *Proc. Natl. Acad. Sci. U.S.A.* **112**, 6887–6891 (2015). doi: 10.1073/pnas.1420232112; pmid: 25964367
- C. Nehrbass-Ahles et al., Abrupt CO₂ release to the atmosphere under glacial and early interglacial climate conditions. *Science* **363**, 1000–1005 (2020). doi: 10.1126/science.aay8178; pmid: 32820127
- C. Le Quéré et al., Trends in the sources and sinks of carbon dioxide. *Nat. Geosci.* **2**, 831–836 (2009). doi: 10.1038/ngeo689
- P. Friedlingstein et al., Global carbon budget 2022. *Earth Syst. Sci. Data* **14**, 4811–4900 (2022). doi: 10.5194/esd-14-4811-2022
- P. Valdes, Built for stability. *Nat. Geosci.* **4**, 414–416 (2011). doi: 10.1038/geo1200
- W. Kiessling, M. Aberhan, L. Villier, Phanerozoic trends in skeletal mineralogy driven by mass extinctions. *Nat. Geosci.* **1**, 527–530 (2008). doi: 10.1038/geo2008251
- J. L. Payne, A. M. Bush, N. A. Heim, M. L. Knipe, D. J. McCauley, Ecological selectivity of the emerging mass extinction in the oceans. *Science* **353**, 1284–1286 (2016). doi: 10.1126/science.aaf2416; pmid: 27629258
- E. J. Edwards et al., The origins of C₄ grasslands: Integrating evolutionary and ecosystem science. *Science* **328**, 587–591 (2010). doi: 10.1126/science.1177216; pmid: 20431008
- F. A. McInerney, S. L. Wing, The Paleocene-Eocene Thermal Maximum: A perturbation of carbon cycle, climate, and biosphere with implications for the future. *Annu. Rev. Earth Planet. Sci.* **39**, 489–516 (2011). doi: 10.1146/annurev-earth-040610-133431
- W. Konrad, D. L. Royer, P. J. Franks, A. Roth-Nebelsick, Quantitative critique of leaf-based paleo-CO₂ proxies: Consequences for their reliability and applicability. *Geol. J.* **56**, 886–902 (2020). doi: 10.1002/gj.3807
- J. C. McElwain, M. Steinhorsdottr, Paleoecology, ploidy, paleoatmospheric composition, and developmental biology: A review of the multiple uses of fossil stomata. *Plant Physiol.* **174**, 650–664 (2017). doi: 10.1104/pp.17.00204; pmid: 28495890
- B. A. Schubert, A. H. Jahren, The effect of atmospheric CO₂ concentration on carbon isotope fractionation in C₃ land plants. *Geochim. Cosmochim. Acta* **96**, 29–43 (2012). doi: 10.1016/j.gca.2012.08.003

25. T. E. Cerling, Carbon dioxide in the atmosphere; evidence from Cenozoic and Mesozoic Paleosols. *Am. J. Sci.* **291**, 377–400 (1991). doi: 10.2475/ajs.291.4.377
26. D. O. Breecker, Quantifying and understanding the uncertainty of atmospheric CO₂ concentrations determined from calcic paleosols. *Geochim. Geophys. Geosyst.* **14**, 3210–3220 (2013). doi: 10.1002/ggge.20189
27. E. A. Jagniecki, T. K. Lowenstein, D. M. Jenkins, R. V. Demicco, Eocene atmospheric CO₂ from the nahcolite proxy. *Geology* **43**, 1075–1078 (2015).
28. T. K. Lowenstein, R. V. Demicco, Elevated Eocene atmospheric CO₂ and its subsequent decline. *Science* **313**, 1928 (2006). doi: 10.1126/science.1129555; pmid: 17008525
29. M. Pagani, “12.13 - Biomarker-based inferences of past climate: The alkenone pCO₂ proxy” in *Treatise on Geochemistry*, vol. 12, H. D. Holland, K. K. Turekian, Eds. (Elsevier, ed. 2, 2014), pp. 361–378. doi: 10.1016/B978-0-08-095975-7.01027-5
30. B. Hönsch et al., *Boron Proxies in Paleoceanography and Paleoclimatology*, Analytical Methods in Earth and Environmental Science Series (John Wiley & Sons, Ltd., 2019).
31. J. W. B. Rae, “Boron isotopes in foraminifera: Systematics, biomineralisation, and CO₂ reconstruction” in *Boron Isotopes: The Fifth Element*, H. Marschall, G. Foster, Eds. (Springer International Publishing, 2018), pp. 107–143. doi: 10.1007/978-3-319-64666-4_5
32. D. J. Beerling, D. L. Royer, Convergent Cenozoic CO₂ history. *Nat. Geosci.* **4**, 418–420 (2011). doi: 10.1038/ngeo1186
33. G. L. Foster, D. L. Royer, D. J. Lunt, Future climate forcing potentially without precedent in the last 420 million years. *Nat. Commun.* **8**, 14845 (2017). doi: 10.1038/ncomms14845; pmid: 28375201
34. J. W. B. Rae et al., Atmospheric CO₂ over the past 66 million years from marine archives. *Annu. Rev. Earth Planet. Sci.* **49**, 609–641 (2021). doi: 10.1146/annurev-earth-082420-063026
35. S. Ji et al., A symmetrical CO₂ peak and asymmetrical climate change during the middle Miocene. *Earth Planet. Sci. Lett.* **499**, 134–144 (2018). doi: 10.1016/j.epsl.2018.07.011
36. J. Da, Y. G. Zhang, G. Li, X. Meng, J. Ji, Low CO₂ levels of the entire Pleistocene epoch. *Nat. Commun.* **10**, 4342 (2019). doi: 10.1038/s41467-019-12357-5; pmid: 31554805
37. E. Hyland, N. D. Sheldon, M. Fan, Terrestrial paleoenvironmental reconstructions indicate transient peak warming during the early Eocene climatic optimum. *Geol. Soc. Am. Bull.* **125**, 1338–1348 (2013). doi: 10.1130/B307611
38. J. Henderiks, M. Pagani, Refining ancient carbon dioxide estimates: Significance of coccolithophore cell size for alkenone-based pCO₂ records. *Paleoceanography* **22**, PA3202 (2007). doi: 10.1029/2006PA001399
39. S. R. Phelps et al., Carbon isotope fractionation in Noelaerhabdaceae algae in culture and a critical evaluation of the alkenone paleobarometer. *Geochim. Geophys. Geosyst.* **22**, e2021GC009657 (2021). doi: 10.1029/2021GC009657
40. H. M. Stoll et al., Uptregulation of phytoplankton carbon concentrating mechanisms during low CO₂ glacial periods and implications for the phytoplankton pCO₂ proxy. *Quat. Sci. Rev.* **208**, 1–20 (2019). doi: 10.1016/j.quascirev.2019.01.012
41. Y. G. Zhang, J. Henderiks, X. Liu, Refining the alkenone-pCO₂ method II: Towards resolving the physiological parameter ‘b’. *Geochim. Cosmochim. Acta* **281**, 118–134 (2020). doi: 10.1016/j.gca.2020.05.002
42. E. G. Hyland, N. D. Sheldon, Coupled CO₂-climate response during the Early Eocene Climatic Optimum. *Palaoclimatol. Palaeoecol.* **369**, 125–135 (2013). doi: 10.1016/j.palaeo.2012.10.011
43. T. Westerhold et al., An astronomically dated record of Earth’s climate and its predictability over the last 66 million years. *Science* **369**, 1383–1387 (2020). doi: 10.1126/science.aba6853; pmid: 32913105
44. J. Hansen, M. Sato, G. Russell, P. Kharecha, Climate sensitivity, sea level and atmospheric carbon dioxide. *Philos. Trans. A Math. Phys. Eng. Sci.* **371**, 20120294 (2013). doi: 10.1098/rsta.2012.0294; pmid: 24043864
45. S. J. Ring, S. G. Mutz, T. A. Ehlers, Cenozoic proxy constraints on earth system sensitivity to greenhouse gases. *Paleoceanogr. Palaeoclimatol.* **37**, e2021PA004364 (2022). doi: 10.1029/2021PA004364
46. T. D. Herbert et al., Late Miocene global cooling and the rise of modern ecosystems. *Nat. Geosci.* **9**, 843–847 (2016). doi: 10.1038/ngeo2813
47. D. E. Gaskell et al., The latitudinal temperature gradient and its climate dependence as inferred from foraminiferal $\delta^{18}\text{O}$ over the past 95 million years. *Proc. Natl. Acad. Sci. U.S.A.* **119**, e2111332119 (2022). doi: 10.1073/pnas.2111332119; pmid: 35254906
48. C. L. O’Brien et al., The enigma of Oligocene climate and global surface temperature evolution. *Proc. Natl. Acad. Sci. U.S.A.* **117**, 25302–25309 (2020). doi: 10.1073/pnas.2003914117; pmid: 32989142
49. D. J. Lunt et al., Palaeogeographic controls on climate and proxy interpretation. *Clim. Past* **12**, 1181–1198 (2016). doi: 10.5194/cp-12-1181-2016
50. A. N. Meckler et al., Cenozoic evolution of deep ocean temperature from clumped isotope thermometry. *Science* **377**, 86–90 (2022). doi: 10.1126/science.abk0604; pmid: 3571913
51. PALAEOSENS Project Members, Making sense of palaeoclimate sensitivity. *Nature* **491**, 683–691 (2012). doi: 10.1038/nature11574; pmid: 2319245
52. A. Tripati, D. Darby, Evidence for ephemeral middle Eocene to early Oligocene Greenland glacial ice and pan-Arctic sea ice. *Nat. Commun.* **9**, 1038 (2018). doi: 10.1038/s41467-018-03180-5; pmid: 2953121
53. H. D. Scher, S. M. Bohaty, B. W. Smith, G. H. Munn, Isotopic interrogation of a suspected late Eocene glaciation. *Paleoceanography* **29**, 628–644 (2014). doi: 10.1002/2014PA002648
54. I. Sauerbreit et al., Gateway-driven weakening of ocean gyres leads to Southern Ocean cooling. *Nat. Commun.* **12**, 6465 (2021). doi: 10.1038/s41467-021-26658-1; pmid: 34753912
55. D. L. Royer, Climate sensitivity in the geologic past. *Annu. Rev. Earth Planet. Sci.* **44**, 277–293 (2016). doi: 10.1146/annurev-earth-100815-024150
56. R. M. Brown, T. B. Chalk, A. J. Crocker, P. A. Wilson, G. L. Foster, Late Miocene cooling coupled to carbon dioxide with Pleistocene-like climate sensitivity. *Nat. Geosci.* **15**, 664–670 (2022). doi: 10.1038/s41561-022-00982-7
57. T. E. Wong, Y. Cui, D. L. Royer, K. Keller, A tighter constraint on Earth-system sensitivity from long-term temperature and carbon-cycle observations. *Nat. Commun.* **12**, 3173 (2021). doi: 10.1038/s41467-021-23543-9; pmid: 34039993
58. D. L. Royer, M. Pagani, D. J. Beerling, Geobiological constraints on Earth system sensitivity to CO₂ during the Cretaceous and Cenozoic. *Geobiology* **10**, 298–310 (2012). doi: 10.1111/j.1472-4669.2012.00320.x; pmid: 22353368
59. J. E. Tierney et al., Spatial patterns of climate change across the Paleocene-Eocene Thermal Maximum. *Proc. Natl. Acad. Sci. U.S.A.* **119**, e2205326119 (2022). doi: 10.1073/pnas.2205326119; pmid: 36215472
60. E. Anagnostou et al., Proxy evidence for state-dependence of climate sensitivity in the Eocene greenhouse. *Nat. Commun.* **11**, 4436 (2020). doi: 10.1038/s41467-020-17887-x; pmid: 32895377
61. J. Hansen et al., Target atmospheric CO: Where should humanity aim? *Open Atmos. Sci. J.* **2**, 217–231 (2008). doi: 10.2174/187428230082010217
62. J. T. Kiehl, C. A. Shields, Sensitivity of the Palaeocene-Eocene Thermal Maximum climate to cloud properties. *Philos. Trans. A Math. Phys. Eng. Sci.* **371**, 20130093 (2013). doi: 10.1098/rsta.2013.0093; pmid: 24043867
63. J. Zhu, C. J. Poulsen, J. E. Tierney, Simulation of Eocene extreme warmth and high climate sensitivity through cloud feedbacks. *Sci. Adv.* **5**, eaax1874 (2019). doi: 10.1126/sciadv.aax1874; pmid: 31555736
64. D. J. Beerling, A. Fox, D. S. Stevenson, P. J. Valdes, Enhanced chemistry-climate feedbacks in past greenhouse worlds. *Proc. Natl. Acad. Sci. U.S.A.* **108**, 9770–9775 (2011). doi: 10.1073/pnas.1102409108; pmid: 21628580
65. T. Schneider, C. M. Kaul, K. G. Pressel, Possible climate transitions from breakup of stratocumulus decks under greenhouse warming. *Nat. Geosci.* **12**, 163–167 (2019). doi: 10.1038/s41561-019-0310-1
66. K. G. Miller et al., Cenozoic sea-level and cryospheric evolution from deep-sea geochemical and continental margin records. *Sci. Adv.* **6**, eaaz1346 (2020). doi: 10.1126/sciadv.aaz1346; pmid: 32440543
67. E. J. Rohling et al., Sea level and deep-sea temperature reconstructions suggest quasi-stable states and critical transitions over the past 40 million years. *Sci. Adv.* **7**, eabf5326 (2021). doi: 10.1126/sciadv.abf5326; pmid: 34172440
68. M. J. Henehan et al., Revisiting the Middle Eocene Climatic Optimum “carbon cycle conundrum” with new estimates of atmospheric pCO₂ from boron isotopes. *Paleoceanogr. Palaeoclimatol.* **35**, e2019PA003713 (2020). doi: 10.1029/2019PA003713
69. E. Gasson et al., Uncertainties in the modelled CO₂ threshold for Antarctic glaciation. *Clim. Past* **10**, 451–466 (2014). doi: 10.5194/cp-10-451-2014
70. R. M. Deconto, Thresholds for Cenozoic bipolar glaciation. *Nature* **455**, 652–656 (2008). doi: 10.1038/nature07337; pmid: 18833277
71. R. M. DeConto, D. Pollard, Rapid Cenozoic glaciation of Antarctica induced by declining atmospheric CO₂. *Nature* **421**, 245–249 (2003). doi: 10.1038/nature01290; pmid: 12529638
72. E. Gasson, R. M. DeConto, D. Pollard, R. H. Levy, Dynamic Antarctic ice sheet during the early to mid-Miocene. *Proc. Natl. Acad. Sci. U.S.A.* **113**, 3459–3464 (2016). doi: 10.1073/pnas.1516130113; pmid: 26903645
73. D. Pollard, R. M. DeConto, Hysteresis in Cenozoic Antarctic ice-sheet variations. *Global Planet. Change* **45**, 9–21 (2005). doi: 10.1016/j.gloplacha.2004.09.011
74. G. J. G. Paxman, E. G. W. Gasson, S. S. R. Jamieson, M. J. Bentley, F. Ferraccioli, Long-term increase in Antarctic Ice Sheet vulnerability driven by bed topography evolution. *Geophys. Res. Lett.* **47**, e2020GL090003 (2020). doi: 10.1029/2020GL090003
75. J. J. Fürst et al., The safety band of Antarctic ice shelves. *Nat. Clim. Chang.* **6**, 479–482 (2016). doi: 10.1038/nclimate2912
76. J. C. McElwain, Paleobotany and global change: Important lessons for species to biomes from vegetation responses to past global change. *Annu. Rev. Plant Biol.* **69**, 761–787 (2018). doi: 10.1146/annurev-plant-042817-040405; pmid: 29719166
77. S. M. Popescu et al., Mangrove distribution and diversity during three Cenozoic thermal maxima in the Northern Hemisphere (pollen records from the Arctic-North Atlantic-Mediterranean regions). *J. Biogeogr.* **48**, 2771–2784 (2021). doi: 10.1111/jbi.14238
78. C. Jaramillo, M. J. Rueda, G. Mora, Cenozoic plant diversity in the neotropics. *Science* **311**, 1893–1896 (2006). doi: 10.1126/science.1121380; pmid: 16574860
79. J. Y. Lim et al., The Cenozoic history of palms: Global diversification, biogeography and the decline of megathermal forests. *Glob. Ecol. Biogeogr.* **31**, 425–439 (2022). doi: 10.1111/geb.13436
80. A. Graham, The age and diversification of terrestrial New World ecosystems through Cretaceous and Cenozoic time. *Am. J. Bot.* **98**, 336–351 (2011). doi: 10.3732/ajb.1000353; pmid: 21613130
81. J. R. Ehleringer, R. K. Monson, Evolutionary and ecological aspects of photosynthetic pathway variation. *Annu. Rev. Ecol. Syst.* **24**, 411–439 (1993). doi: 10.1146/annurev.es.24.110193.002211
82. H. Griffiths, “Carbon dioxide concentrating mechanisms and the evolution of CAM in vascular epiphytes” in *Vascular Plants as Epiphytes: Evolution and Ecophysiology*, U. Lüttge, Ed. (Springer, 1989), pp. 42–86. doi: 10.1007/978-3-642-74465-5_3
83. C. J. Still, J. A. Berry, G. J. Collatz, R. S. DeFries, Global distribution of C₃ and C₄ vegetation: Carbon cycle implications. *Global Biogeochem. Cycles* **17**, 1006 (2003). doi: 10.1029/2001GB001807
84. P.-A. Christin et al., Oligocene CO₂ decline promoted C₄ photosynthesis in grasses. *Curr. Biol.* **18**, 37–43 (2008). doi: 10.1016/j.cub.2007.11.058; pmid: 18160293
85. A. Vicentini, J. C. Barber, S. S. Aliscioni, L. M. Giussani, E. A. Kellogg, The age of the grasses and clusters of origins of C₄ photosynthesis. *Glob. Change Biol.* **14**, 2963–2977 (2008). doi: 10.1111/j.1365-2486.2008.01688.x
86. P. J. Polissar, C. Rose, K. T. Uno, S. R. Phelps, P. deMenocal, Synchronous rise of African C₄ ecosystems 10 million years ago in the absence of aridification. *Nat. Geosci.* **12**, 657–660 (2019). doi: 10.1038/s41561-019-0399-2
87. L. Tauxe, S. J. Feakins, A reassessment of the chronostratigraphy of late Miocene C₃–C₄ transitions. *Paleoceanogr. Palaeoclimatol.* **35**, e2020PA003857 (2020). doi: 10.1029/2020PA003857
88. T. E. Cerling et al., Global vegetation change through the Miocene/Pliocene boundary. *Nature* **389**, 153–158 (1997). doi: 10.1038/38229
89. M. Arakaki et al., Contemporaneous and recent radiations of the world’s major succulent plant lineages. *Proc. Natl. Acad.*

- Sci. U.S.A.* **108**, 8379–8384 (2011). doi: [10.1073/pnas.1100628108](https://doi.org/10.1073/pnas.1100628108); pmid: [21536881](https://pubmed.ncbi.nlm.nih.gov/21536881/)
90. T. J. Givnish *et al.*, Orchid phylogenomics and multiple drivers of their extraordinary diversification. *Proc. Biol. Sci.* **282**, 20151553 (2015). doi: [10.1098/rspb.2015.1553](https://doi.org/10.1098/rspb.2015.1553); pmid: [26311671](https://pubmed.ncbi.nlm.nih.gov/26311671/)
91. E. J. Edwards, Evolutionary trajectories, accessibility and other metaphors: The case of C₄ and CAM photosynthesis. *New Phytol.* **223**, 1742–1755 (2019). doi: [10.1111/nph.15851](https://doi.org/10.1111/nph.15851); pmid: [30993711](https://pubmed.ncbi.nlm.nih.gov/30993711/)
92. J. R. Ehleringer, T. E. Cerling, B. R. Helliker, C₄ photosynthesis, atmospheric CO₂, and climate. *Oecologia* **112**, 285–299 (1997). doi: [10.1007/s004420050311](https://doi.org/10.1007/s004420050311); pmid: [28307475](https://pubmed.ncbi.nlm.nih.gov/28307475/)
93. H. Zhou, B. R. Helliker, M. Huber, A. Dicks, E. Akçay, C₄ photosynthesis and climate through the lens of optimality. *Proc. Natl. Acad. Sci. U.S.A.* **115**, 12057–12062 (2018). doi: [10.1073/pnas.1718981115](https://doi.org/10.1073/pnas.1718981115); pmid: [30401739](https://pubmed.ncbi.nlm.nih.gov/30401739/)
94. C. E. R. Lehmann, S. A. Archibald, W. A. Hoffmann, W. J. Bond, Deciphering the distribution of the savanna biome. *New Phytol.* **191**, 197–209 (2011). doi: [10.1111/j.1469-8137.2011.03689.x](https://doi.org/10.1111/j.1469-8137.2011.03689.x); pmid: [21463328](https://pubmed.ncbi.nlm.nih.gov/21463328/)
95. W. M. Kürschner, Z. Vracek, D. L. Dilcher, The impact of Miocene atmospheric carbon dioxide fluctuations on climate and the evolution of terrestrial ecosystems. *Proc. Natl. Acad. Sci. U.S.A.* **105**, 449–453 (2008). doi: [10.1073/pnas.0708581105](https://doi.org/10.1073/pnas.0708581105); pmid: [18174330](https://pubmed.ncbi.nlm.nih.gov/18174330/)
96. C. A. E. Strömborg, Evolution of grasses and grassland ecosystems. *Annu. Rev. Earth Planet. Sci.* **39**, 517–544 (2011). doi: [10.1146/annurev-earth-040809-152402](https://doi.org/10.1146/annurev-earth-040809-152402)
97. A. T. Karp, K. T. Uno, P. J. Polisar, K. H. Freeman, Late Miocene C₄ grassland fire feedbacks on the Indian subcontinent. *Paleoceanogr. Paleoclimatol.* **36**, e2020PA004106 (2021). doi: [10.1029/2020PA004106](https://doi.org/10.1029/2020PA004106)
98. T. Tukula *et al.*, Drier winters drove Cenozoic paleohabitat expansion in North America. *AGU Adv.* **3**, e2021AV000566 (2022). doi: [10.1029/2021AV000566](https://doi.org/10.1029/2021AV000566)
99. M. Fortelius *et al.*, Evolution of Neogene mammals in Eurasia: Environmental forcing and biotic interactions. *Annu. Rev. Earth Planet. Sci.* **42**, 579–604 (2014). doi: [10.1146/annurev-earth-050212-124030](https://doi.org/10.1146/annurev-earth-050212-124030)
100. F. Kaya *et al.*, The rise and fall of the Old World savannah fauna and the origins of the African savannah biome. *Nat. Ecol. Evol.* **2**, 241–246 (2018). doi: [10.1038/s41559-017-04141-1](https://doi.org/10.1038/s41559-017-04141-1); pmid: [29292396](https://pubmed.ncbi.nlm.nih.gov/29292396/)
101. C. M. Janis, J. Damuth, J. M. Theodor, Miocene ungulates and terrestrial primary productivity: Where have all the browsers gone? *Proc. Natl. Acad. Sci. U.S.A.* **97**, 7899–7904 (2000). doi: [10.1073/pnas.97.14.7899](https://doi.org/10.1073/pnas.97.14.7899); pmid: [10884422](https://pubmed.ncbi.nlm.nih.gov/10884422/)
102. M. Fortelius, N. Solounias, Functional characterization of ungulate molars using the abrasion-attrition wear gradient: A new method for reconstructing paleodiets. *Am. Mus. Novit.* **3301**, 1–36 (2000). doi: [10.1206/0003-0082\(2000\)3301-0001:FCOMU>2.0.CO;2](https://doi.org/10.1206/0003-0082(2000)3301-0001:FCOMU>2.0.CO;2)
103. M. C. Mihlbachler, F. Rivals, N. Solounias, G. M. Semprebon, Dietary change and evolution of horses in North America. *Science* **331**, 1178–1181 (2011). doi: [10.1126/science.1196166](https://doi.org/10.1126/science.1196166); pmid: [21385712](https://pubmed.ncbi.nlm.nih.gov/21385712/)
104. C. A. E. Strömborg, Evolution of hypodonty in equids: Testing a hypothesis of adaptation. *Paleobiology* **32**, 236–258 (2006). doi: [10.1666/0094-8373\(2006\)32\[236:EOHET\]2.0.CO;2](https://doi.org/10.1666/0094-8373(2006)32[236:EOHET]2.0.CO;2)
105. C. M. Janis, M. Fortelius, On the means whereby mammals achieve increased functional durability of their dentitions, with special reference to limiting factors. *Biol. Rev. Camb. Philos. Soc.* **63**, 197–230 (1988). doi: [10.1111/j.1469-185X.1988.tb00630.x](https://doi.org/10.1111/j.1469-185X.1988.tb00630.x); pmid: [3042033](https://pubmed.ncbi.nlm.nih.gov/3042033/)
106. M. R. Badger, D. Hanson, G. D. Price, Evolution and diversity of CO₂ concentrating mechanisms in cyanobacteria. *Funct. Plant Biol.* **29**, 161–173 (2002). doi: [10.1071/PP01213](https://doi.org/10.1071/PP01213); pmid: [12689463](https://pubmed.ncbi.nlm.nih.gov/12689463/)
107. M. P. S. Badger, Alkenone isotopes show evidence of active carbon concentrating mechanisms in coccolithophores as aqueous carbon dioxide concentrations fall below 7 μmol L⁻¹. *Biogeosciences* **18**, 1149–1160 (2021). doi: [10.5194/bg-18-1149-2021](https://doi.org/10.5194/bg-18-1149-2021)
108. Y. G. Zhang, M. Pagani, Z. Liu, S. M. Bohaty, R. Deconto, A 40-million-year history of atmospheric CO₂. *Philos. Trans. A Math. Phys. Eng. Sci.* **371**, 20130096 (2013). doi: [10.1098/rsta.2013.0096](https://doi.org/10.1098/rsta.2013.0096); pmid: [24043869](https://pubmed.ncbi.nlm.nih.gov/24043869/)
109. P. D. Tortell, Evolutionary and ecological perspectives on carbon acquisition by phytoplankton. *Limnol. Oceanogr.* **45**, 744–750 (2000). doi: [10.4319/lo.2000.45.3.00744](https://doi.org/10.4319/lo.2000.45.3.00744)
110. C. T. Bolton, H. M. Stoll, Late Miocene threshold response of marine algae to carbon dioxide limitation. *Nature* **500**, 558–562 (2013). doi: [10.1038/nature12448](https://doi.org/10.1038/nature12448); pmid: [23985873](https://pubmed.ncbi.nlm.nih.gov/23985873/)
111. M. N. Evans, S. E. Tolwinski-Ward, D. M. Thompson, K. J. Anchukaitis, Applications of proxy system modeling in high resolution paleoclimate. *Quat. Sci. Rev.* **76**, 16–28 (2013). doi: [10.1016/j.quascirev.2013.05.024](https://doi.org/10.1016/j.quascirev.2013.05.024)
112. G. J. Bowen, B. Fischer-Femal, G. J. Reichart, A. Sluijs, C. H. Lear, Joint inversion of proxy system models to reconstruct paleoenvironmental time series from heterogeneous data. *Clim. Past* **16**, 65–78 (2020). doi: [10.5194/cp-16-65-2020](https://doi.org/10.5194/cp-16-65-2020)
113. M. B. Osman *et al.*, Globally resolved surface temperatures since the Last Glacial Maximum. *Nature* **599**, 239–244 (2021). doi: [10.1038/s41586-021-03984-4](https://doi.org/10.1038/s41586-021-03984-4); pmid: [34759364](https://pubmed.ncbi.nlm.nih.gov/34759364/)
114. C. Godbillot, F. Minoletti, F. Bassinot, M. Hermoso, Parallel between the isotopic composition of coccolith calcite and carbon levels across Termination II: developing a paleo-CO₂ probe. *Clim. Past* **18**, 449–464 (2022). doi: [10.5194/cp-18-449-2022](https://doi.org/10.5194/cp-18-449-2022)
115. A. Pack, A. Gehler, A. Süssenberger, Exploring the usability of isotopically anomalous oxygen in bones and teeth as paleo-CO₂-barometer. *Geochim. Cosmochim. Acta* **102**, 306–317 (2013). doi: [10.1016/j.gca.2012.10.017](https://doi.org/10.1016/j.gca.2012.10.017)
116. C. R. Scotese, An atlas of Phanerozoic paleogeographic maps: the seas come in and the seas go out. *Annu. Rev. Earth Planet. Sci.* **49**, 679–728 (2021). doi: [10.1146/annurev-earth-081320-064052](https://doi.org/10.1146/annurev-earth-081320-064052)
117. P. A. Christin, C. P. Osborne, R. F. Sage, M. Arakaki, E. J. Edwards, C₄ eu dicots are not younger than C₄ monocots. *J. Exp. Bot.* **62**, 3171–3181 (2011). doi: [10.1093/jxb/err041](https://doi.org/10.1093/jxb/err041); pmid: [21933833](https://pubmed.ncbi.nlm.nih.gov/21933833/)
- ACKNOWLEDGMENTS**
- We thank C. Major at NSF and the many researchers who contributed advice and enthusiasm for this project over the years. We are grateful to the staff at the National Centers for Environmental Information (NCEI) for facilitating curation of the paleo-CO₂ database, and to LDEO, the UCLA Lake Arrowhead Lodge, and the Lady Bird Johnson Wildflower Center for hosting the three workshops that framed this work. Two anonymous reviewers provided valuable comments that improved this manuscript. This study is dedicated to Wally Broecker and Taro Takahashi, who pioneered the study of CO₂ dynamics in a changing climate. **Funding:** This work was supported by National Science Foundation grant OCE 16-36005 (B.H. and P.J.P.), Heising-Simons Foundation grant 2018-0996 (B.H. and V.F.), National Science Foundation grant EAR 21-21649 (B.H., V.F., J.J.M., and C.F.G.), National Science Foundation grant EAR 21-2170 (G.J.B.), National Science Foundation grant 20-02370 (Y.C.), National Science Foundation grant 18-43285 (A.P.), Columbia University's Center for Climate and Life (K.T.U.), the G. Unger Vetlesen Foundation (K.T.U.), National Science Foundation grant 21-00537 (A.P. and P.J.P.), National Science Foundation grant 21-00509 (P.J.P.), National Science Foundation grant EAR 21-21165 (A.R.), National Science Foundation grant EAR 18-06015 (Y.G.Z.), National Science Foundation grant DGE 16-44869 (S.R.P.), National Science Foundation grant 18-13703 (E.G.H.), National Science Foundation grant OCE 16-58023 (J.C.Z.), National Science Foundation grant 16-02905 (M.H.), Swedish Research Council grant NT7-2016 04905 (M.S.), European Research Council grant 101020824 (J.C.M.), SFI/RC/2092 (J.C.M.), UK Research and Innovation grant 101045371 (M.J.H.), Natural Environment Research Council grant NE/X000567/1 (M.P.S.B.), Royal Society grant DHF/RN/221014 (C.R.W.), Australian Research Council grant DP150104007 (P.J.F.), Deutsche Forschungsgemeinschaft grant RA 2068/4-1 (M.R.), European Research Council grant 805246 (J.W.B.R.), an ETH Fellowship (J.K.C.R.), National Science Foundation of China grant 42030503 (J.D.), the Sandia Society Museum (G.J.R.), a Royal Society Tata Fellowship (B.D.A.N.), and Natural Environment Research Council grant NE/P019048/1 (G.L.F.). **Author contributions:** Conceptualization: B.H., G.J.B., D.O.B., M.J.H., A.P., P.J.P., S.R.P., A.R., D.L.R., M.S., R.S.B., P.J.F., M.H., M.F.S., J.K.C.R., N.D.S., and Y.G.Z. Data curation: B.H., G.J.B., D.O.B., Y.C., M.J.H., M.J.K., J.C.M., P.J.P., D.L.R., M.S., S.R.P., E.A., M.P.S.B., R.S.B., T.B.C., E.d.I.V., K.A.D., C.F.G., M.Gut., D.T.H., L.L.H., T.K.L., M.Gui., J.N.M., R.W., A.R.-N., M.F.S., N.D.S., S.S., C.R.W., Y.G.Z., J.M.C., J.D., D.D.E., G.L.F., E.G.H., B.D.A.N., J.W.B.R., M.R., G.J.R., O.S., and L.Z. Formal analysis: B.H., G.J.B., D.O.B., Y.C., M.J.H., P.J.P., D.L.R., A.M., and C.E.L. Investigation: B.H., D.O.B., P.J.P., S.R.P., G.J.B., M.J.H., Y.C., J.C.M., M.J.K., A.P., E.A., M.P.S.B., R.S.B., P.J.F., W.K., T.K.L., M.F.S., and Y.G.Z. Software: G.J.B., V.F., J.J.M., and R.W. Visualization: B.H., G.J.B., M.J.H., M.S., J.C.M., K.T.U., P.J.P., D.O.B., J.A., B.A.K., C.R.S., J.J.M., and R.W. Funding acquisition: B.H., P.J.P., D.L.R., D.O.B., G.J.B., M.J.K., A.P., R.M.D., M.H., K.E.S., and V.F. Project administration: B.H., D.L.R., D.O.B., P.J.P., and G.J.B. Writing – original draft: B.H., D.L.R., D.O.B., P.J.P., G.J.B., M.J.H., Y.C., M.S., J.C.M., M.J.K., A.P., K.T.U., A.R., and S.R.P. Writing – review & editing: All authors. **Competing interests:** The authors have no competing interests to declare. **Data and materials availability:** The completed data sheets for each study can be accessed as the paleo-CO₂ “Archive” at NOAA’s NCEI (https://www.ncdc.noaa.gov/pub/data/paleo/climate_forcing/trace_gases/Paleo-pCO2/). The specific choice of category, as well as the updated CO₂ and age estimates, are documented in “Product” sheets for each dataset and proxy. In contrast to the “Archive,” which will grow with new publications but will otherwise remain passive, the paleo-CO₂ “Product” is a living database that will be updated when newly published data or ancillary data constraints become available and/or when methodological improvements are developed that enable modernization of previously underconstrained datasets. The “Product” sheets created for this study can be accessed at NCEI (https://www.ncei.noaa.gov/pub/data/paleo/climate_forcing/trace_gases/Paleo-pCO2/product_files/), and this is also the place where future data updates will be made available in consecutive versions of the data “Product.” **License information:** Copyright © 2023 the authors, some rights reserved; exclusive licensee American Association for the Advancement of Science. No claim to original US government works. <https://www.science.org/about/science-licenses-journal-article-reuse>
- The CenCO₂PIP Consortium**
- Bärbel Höönisch^{1,2}, Dana L. Royer³, Daniel O. Breecker⁴, Pratigya O. Polissar⁵, Gabriel J. Bowen⁶, Michael J. Henehan⁷, Ying Cui⁸, Margaret Steinthorsdottir⁹, Jennifer C. McElwain¹⁰, Matthew J. Kohn¹¹, Ann Pearson¹², Samuel R. Phelps¹³, Kevin T. Uno², Andy Ridgewell¹⁴, Eleni Anagnostou¹⁵, Jacqueline Austermaier¹², Marcus P. S. Badger¹⁶, Richard S. Barclay¹⁷, Peter K. Bijls¹⁸, Thomas B. Chalk¹⁹, Christopher R. Scotese²⁰, Elwyn de la Vega²¹, Robert M. DeConto²², Kelsey A. Dyez²³, Vicki Ferrini², Peter J. Franks²⁴, Claudia F. Giulivi², Marcus Gutjahr¹⁵, Dustin T. Harper⁶, Laura L. Haynes²⁵, Matthew Huber²⁶, Kathryn E. Snell²⁷, Benjamin A. Keisling²⁸, Wilfried Konrad²⁹, Tim K. Lowenstein³⁰, Alberto Malinverno², Maxence Guillermic³¹, Luz María Mejía³², Joseph N. Milligan¹⁷, John J. Morton², Lee Nord³³, Ross Whiteford³⁴, Anita Roth-Nebelsick³⁵, Jeremy K. C. Rogeneggen³⁶, Morgan F. Schaller³⁷, Nathan D. Sheldon²³, Sindia Sosdian³⁸, Elise B. Wilkes³⁹, Caitlyn R. Witkowski⁷, Yi Ge Zhang⁴⁰, Lloyd Anderson^{1,2}, David J. Beerling⁴¹, Clara Bolton¹⁹, Thure Erle Cerling⁶, Jennifer M. Cotton⁴², Jiawei Da⁴⁴, Douglas D. Ekart⁴³, Gavin L. Foster⁴⁴, David R. Greenwood⁴⁵, Ethan H. Hyland⁴⁶, Elliott A. Jagniecki⁴⁷, John P. Jasper⁴⁸, Jennifer B. Kowalczyk⁴⁹, Lutz Kunzmann⁵⁰, Wolfram M. Kürschner⁵¹, Charles E. Lawrence⁵², Caroline H. Lear³⁸, Miguel A. Martínez-Bot^{44,53}, Daniel P. Maxbauer⁵⁴, Paolo Montagna⁵⁵, B. David A. Naafs⁵⁶, James W. B. Rae³⁴, Markus Raitzsch⁵⁷, Gregory J. Retallack⁵⁸, Simon J. Ring⁵⁹, Osamu Seki⁵⁰, Julio Sepúlveda⁶¹, Ashish Sinha⁶², Tekie F. Tesfamichael⁶³, Aradhna Tripathi³¹, Johan van der Burgh⁶⁴, Jimin Yu⁶⁵, James C. Zachos⁶⁶, Laiming Zhang⁶⁷
- ¹Department of Earth and Environmental Sciences of Columbia University, New York, NY, USA. ²Lamont-Doherty Earth Observatory of Columbia University, Palisades, NY, USA. ³Department of Earth and Environmental Sciences, Wesleyan University, Middletown, CT, USA. ⁴Department of Earth and Planetary Sciences, Jackson School of Geosciences, University of Texas at Austin, Austin, TX, USA. ⁵Department of Ocean Sciences, University of California, Santa Cruz, Santa Cruz, CA, USA. ⁶Department of Geology and Geophysics, University of Utah, Salt Lake City, UT, USA. ⁷School of Earth Sciences, University of Bristol, Bristol, UK. ⁸Department of Earth and Environmental Studies, Montclair State University, Montclair, NJ, USA. ⁹Swedish Museum of Natural History, Stockholm, Sweden. ¹⁰Department of Botany, Trinity College Dublin, Dublin, Ireland. ¹¹Department of Geosciences, Boise State University, Boise, ID, USA. ¹²Department of Earth and Planetary Sciences, Harvard University, Cambridge, MA, USA. ¹³CIM Group, New York, NY, USA. ¹⁴Earth and Planetary Sciences Department, University of California, Riverside, Riverside, CA, USA. ¹⁵GEOMAR Helmholtz Centre for Ocean Research Kiel, Kiel, Germany. ¹⁶School of Environment, Earth and Ecosystem Sciences, The Open University, Milton Keynes, UK. ¹⁷Department of Paleobiology, Smithsonian Institution, Washington, DC, USA. ¹⁸Department of Earth Sciences, Utrecht University, Utrecht, Netherlands. ¹⁹Aix Marseille University, CNRS, IRD, INRAE, CEREGE, Aix-en-Provence, France. ²⁰Department of Earth and Planetary Sciences, Northwestern University, Evanston, IL, USA. ²¹School of Geography, Archaeology and Irish Studies, University of Galway, Ollscoil na Gaillimhe, Galway, Ireland. ²²Department of

Earth, Geographic, and Climate Sciences, University of Massachusetts, Amherst, MA, USA. ²³Department of Earth and Environmental Sciences, University of Michigan, Ann Arbor, MI, USA. ²⁴School of Life and Environmental Sciences, The University of Sydney, Sydney, Australia. ²⁵Department of Earth Science and Geography, Vassar College, Poughkeepsie, NY, USA. ²⁶Department of Earth, Atmospheric, and Planetary Sciences, Purdue University, West Lafayette, IN, USA. ²⁷Department of Geological Sciences, University of Colorado Boulder, Boulder, CO, USA. ²⁸University of Texas Institute for Geophysics, Austin, TX, USA. ²⁹Department of Geosciences, University of Tübingen, Tübingen, Germany. ³⁰Department of Earth Sciences, Binghamton University, Binghamton, NY, USA. ³¹Department of Earth, Planetary and Space Sciences, University of California, Los Angeles, Los Angeles, CA, USA. ³²MARUM, University of Bremen, Bremen, Germany. ³³Department of Geosciences, Baylor University, Waco, TX, USA. ³⁴School of Earth and Environmental Sciences, University of St Andrews, St Andrews, UK. ³⁵State Museum of Natural History, Stuttgart, Germany. ³⁶Department of Geosciences, Colorado State University, Fort Collins, CO, USA. ³⁷Department of Earth and Environmental Sciences, Rensselaer Polytechnic Institute, Troy, NY, USA. ³⁸School of Earth and Environmental Sciences, Cardiff University, Cardiff, UK. ³⁹Ginkgo Bioworks, Boston, MA, USA.

⁴⁰Department of Oceanography, Texas A&M University, College Station, TX, USA. ⁴¹School of Biosciences, University of Sheffield, Sheffield, UK. ⁴²Department of Geological Science, California State University, Northridge, Northridge, CA, USA. ⁴³Department of Earth Science, Utah Valley University, Orem, UT, USA. ⁴⁴School of Ocean and Earth Science, National Oceanography Centre, University of Southampton, Southampton, UK. ⁴⁵Department of Biology, Brandon University, Brandon, Manitoba, Canada. ⁴⁶Department of Marine, Earth, and Atmospheric Sciences, North Carolina State University, Raleigh, NC, USA. ⁴⁷Utah Geological Survey, Salt Lake City, UT, USA. ⁴⁸Nature's Fingerprint Authentication, Molecular Isotope Technologies, LLC, Niantic, CT, USA. ⁴⁹Department of Earth, Environmental and Planetary Sciences, Brown University, Providence, RI, USA. ⁵⁰Senckenberg Natural History Collections, Dresden, Germany. ⁵¹Department of Geosciences, University of Oslo, Oslo, Norway. ⁵²Department of Applied Mathematics, Brown University, Providence, RI, USA. ⁵³EIT Urban Mobility, Barcelona, Spain. ⁵⁴Department of Geology, Carleton College, Northfield, MN, USA. ⁵⁵Institute of Polar Sciences—National Research Council, Bologna, Italy. ⁵⁶School of Chemistry, University of Bristol, Bristol, UK. ⁵⁷Dettmer Group KG, Bremen, Germany. ⁵⁸Department of Earth Sciences, University of Oregon, Eugene, OR, USA. ⁵⁹Deutsches GeoForschungsZentrum GFZ, Potsdam, Germany.

⁶⁰Institute of Low Temperature Science, Hokkaido University, Sapporo, Japan. ⁶¹Department of Geological Sciences and Institute of Arctic and Alpine Research, University of Colorado Boulder, Boulder, CO, USA. ⁶²Department of Earth Science, California State University, Dominguez Hills, Carson, CA, USA. ⁶³School of Earth Sciences, Addis Ababa University, Addis Ababa, Ethiopia. ⁶⁴Independent researcher, Rossum, Netherlands. ⁶⁵Laoshan Laboratory, Qingdao, China. ⁶⁶Department of Earth and Planetary Sciences, University of California, Santa Cruz, Santa Cruz, CA, USA. ⁶⁷Frontiers Science Center for Deep-time Digital Earth, School of Earth Sciences and Resources, China University of Geosciences (Beijing), Beijing, China.

SUPPLEMENTARY MATERIALS

science.org/doi/10.1126/science.adl5177

Supplementary Text

Figs. S1 to S13

Tables S1 to S3

References ([118–439](#))

Submitted 2 May 2023; accepted 30 October 2023

10.1126/science.adl5177